# Chapter 3

# Finite element simulations at the microscopic level

[1] Finite element simulations are an efficient homogenization method in terms of accuracy. For this, a RVE or unit cell must be defined, meshed and loaded so that the final response can be computed. All these aspects are examined in this chapter for different unit cells: 2D, 2D axisymmetric and 3D ones.

## 3.1 Two-dimensional unit cells

In some cases, three-dimensional geometries can be represented by two-dimensional unit cells. Two possibilities are considered here: composite reinforced by aligned fibers and axisymmetric geometries.

### 3.1.1 Composites reinforced by long fibers

For composites reinforced by aligned long fibers, the knowledge of the geometry of a cross section perpendicular to the fibers is enough. This geometry is described by the arrangements of the fibers within the matrix. Two possibilities will be examined in the numerical section: square and hexagonal array of fibers (see figure 3.1). Of course, in order to model the long fibers, plane strain (i.e. deformation in the longitudinal direction is zero) or generalized plane strain (i.e. deformation in the longitudinal direction is constant) elements are used. With the help of the symmetries, the dashed unit cell can be reduced to only one quarter of it (continuous lines of figure 3.1). If the cell periodicity

[1] Some developments of this chapter led to the publication "Micromechanics of elasto-plastic materials reinforced with ellipsoidal inclusions", Pierard O., González C., Segurado J., LLorca J. and Doghri I., *Mechanics of Materials*, submitted for publication [81].

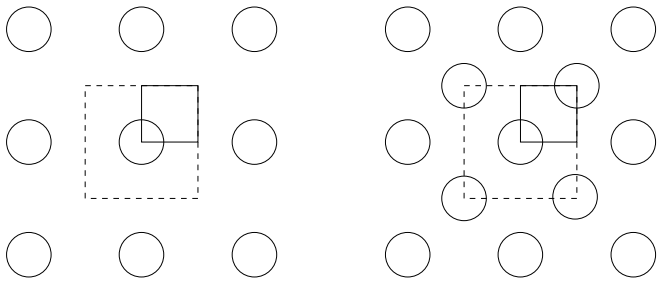

(a) Square arrangement of fibers.

(b) Hexagonal arrangement of fibers.

Figure 3.1: Unit cells with different arrangements of fibers.

is required (e.g.: asymptotic homogenization or prescribed periodic boundary conditions over the unit cell), symmetries cannot be taken into account and only the entire unit cell can be considered. A main limitation of using 2D unit cells to represent 3D geometries is that it is not possible to simulate all the loading possibilities (e.g.: shear in the longitudinal direction). It is well known that the considered unit cell might have a significant impact on the global response, especially in the non-linear regime (see Hom [44], Doghri and Friebel [25]). Several authors have already discussed this subject, e.g. Böhm and Han [9] for two-phase isothermal composites and Weissenbek *et al.* [104] for two-phase thermo-elastic(-plastic) composites. Tucker and Liang [100] also made various FE calculations based on different unit cells. This is illustrated on several examples in the different numerical simulation sections of this work (e.g.: section 5.4.1).

### 3.1.2 Two-dimensional axisymmetric unit cells

As done in several works (e.g.: Christman *et al.* [20], LLorca and Segurado [64]), a classical approach is an approximation of the 3D microstructure by a 2D axisymmetric unit cell as illustrated on figure 3.2. Space is supposed filled by prisms with a hexagonal basis which represent the matrix, each prism being reinforced by a spherical inclusion in its middle. To take advantage of symmetry of the unit cell, the prism is approximated by a cylinder. The unit cell can then be reduced to a 2D axisymmetric one.

Boundary conditions for a uniaxial tension test are the following. For symmetry reasons, no vertical (axial) displacement is allowed on bottom side (1 on figure 3.2) and no horizontal (radial) one on the left side (3). Also, the right side (4) must remain vertical, so that all the horizontal displacements are the same. Displacements are imposed gradually on the top side (2) to reach the required strain at the end of the simulation. Three-node linear axisymmetric

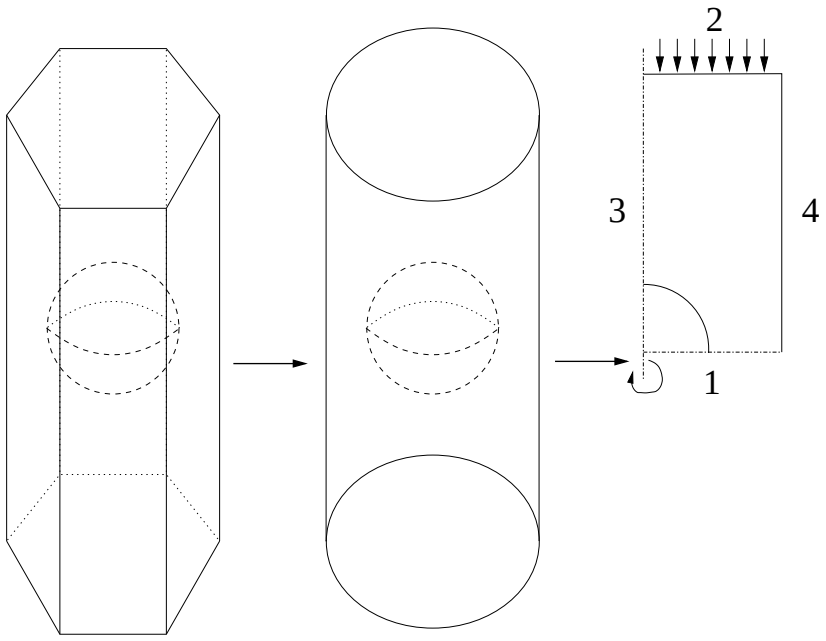


Figure 3.2: Reduction to a 2D axisymmetric unit cell of a sphere-reinforced composite material.

triangles (CAX3 in ABAQUS [1]) or six-node quadratic axisymmetric triangles (CAX6) are used to mesh the surface and about 10000 elements give a sufficiently refined mesh.

### 3.1.3 Boundary conditions

In section 2.2.2, various boundary conditions to the boundary value problem over the RVE have been presented which include uniform traction, linear displacement and periodic boundary conditions. This section explains how to use these boundary conditions with the FE method. Also, prediction of the macroscopic response can be done in a more efficient way than from a volume average of the fields as in (2.2) or (2.4).

#### Linear displacement boundary conditions

If linear displacements are applied on the boundary, the macroscopic stress response can be computed from a volume average of the stress tensor given at

each integration point over the volume:

$$\bar{\boldsymbol{\sigma}} = \frac{1}{V} \sum_{k=1}^{k=N_k} \boldsymbol{\sigma}_k \, V_k, \tag{3.1}$$

where $\boldsymbol{\sigma}_k$ is the stress acting at the integration point $k$, $V_k$ is the representative volume of the integration point $k$ and $N_k$ is the number of integration points within the volume.

More simply, with the help of (2.5), this can be computed by an average of the resulting tractions acting on the boundary:

$$\bar{\boldsymbol{\sigma}} = \frac{1}{V} \sum_{p=1}^{p=N_p} \boldsymbol{t}_p \otimes \boldsymbol{x}_p, \tag{3.2}$$

where $N_p$ is the number of nodes over the boundary of the RVE, $\boldsymbol{t}_p$ are the resulting tractions at node $p$ and $\boldsymbol{x}_p$ is the position vector at this node.

In the case of a uniaxial tensile test in direction 1, the macroscopic normal stress component in this direction becomes:

$$\bar{\sigma}_{11} = \frac{1}{S} \sum_{p=1}^{p=N_{p_1}} t_1, \tag{3.3}$$

where $S$ is the area of the surface on which tractions are imposed and $N_{p_1}$ is the number of nodes lying on that surface.

### Uniform traction boundary conditions

If uniform tractions are applied, the macroscopic strain response can also be computed either from a volume average of the strain tensor given at all the integration points over the volume:

$$\bar{\boldsymbol{\varepsilon}} = \frac{1}{V} \sum_{k=1}^{k=N_k} \boldsymbol{\varepsilon}_k V_k. \tag{3.4}$$

Equivalently, with the help of (2.3), this can be computed by an an average of the resulting displacements on the boundary:

$$\bar{\boldsymbol{\varepsilon}} = \frac{1}{2V} \sum_{p=1}^{p=N_p} (\boldsymbol{u}_p \otimes \boldsymbol{n}_p + \boldsymbol{n}_p \otimes \boldsymbol{u}_p), \tag{3.5}$$

where $\boldsymbol{u}_p$ is the resulting displacement at the boundary node $p$ and $\boldsymbol{n}_p$ is the normal vector to the boundary at this node.

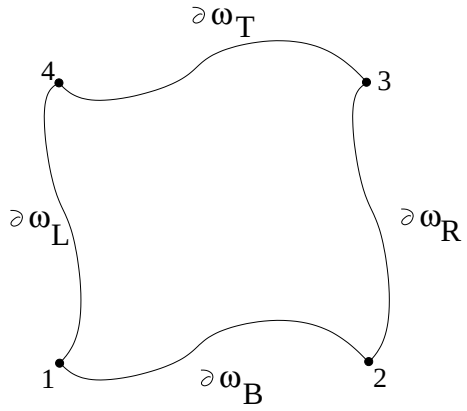


Figure 3.3: Definition of the boundaries, master node (node 1) and slave nodes (nodes 2 and 4) for periodic boundary conditions used in the FE method.

### Periodic boundary conditions

**Application of the conditions** In addition to the microstructural periodicity, meshes are supposed to be the same on opposite faces so that initial positions of every corresponding pair of nodes are related through (see figure 3.3 for notations):

$$\begin{aligned} \boldsymbol{x}_R - \boldsymbol{x}_L &= \boldsymbol{x}_2 - \boldsymbol{x}_1, \\ \boldsymbol{x}_T - \boldsymbol{x}_B &= \boldsymbol{x}_4 - \boldsymbol{x}_1, \end{aligned} \tag{3.6}$$

where $\boldsymbol{x}_s$ lies on $\partial\omega_s$, $s = R, L, T, B$. $\boldsymbol{x}_1$ is the master node and $\boldsymbol{x}_2$ and $\boldsymbol{x}_4$ are the slave nodes. With the help of equation (2.11) and for a given macroscopic strain $\bar{\boldsymbol{\varepsilon}}$ ($\bar{\boldsymbol{\varepsilon}} = \frac{1}{2}(\bar{\boldsymbol{G}} + \bar{\boldsymbol{G}}^T)$), this can be rewritten in term of displacements as:

$$\begin{aligned} \boldsymbol{u}_R - \boldsymbol{u}_L &= \bar{\boldsymbol{G}}.(\boldsymbol{x}_R - \boldsymbol{x}_L) = \bar{\boldsymbol{G}}.(\boldsymbol{x}_2 - \boldsymbol{x}_1), \\ \boldsymbol{u}_T - \boldsymbol{u}_B &= \bar{\boldsymbol{G}}.(\boldsymbol{x}_T - \boldsymbol{x}_B) = \bar{\boldsymbol{G}}.(\boldsymbol{x}_4 - \boldsymbol{x}_1). \end{aligned} \tag{3.7}$$

If following displacements are applied to the master and slave nodes:

$$\boldsymbol{u}_1 = \bar{\boldsymbol{G}}.\boldsymbol{x}_1, \tag{3.8}$$

$$\boldsymbol{u}_2 = \bar{\boldsymbol{G}}.\boldsymbol{x}_2, \tag{3.9}$$

$$\boldsymbol{u}_4 = \bar{\boldsymbol{G}}.\boldsymbol{x}_4, \tag{3.10}$$

periodic boundary conditions may be rewritten as:

$$\boldsymbol{u}_R - \boldsymbol{u}_L = \boldsymbol{u}_2 - \boldsymbol{u}_1, \tag{3.11}$$

$$\boldsymbol{u}_T - \boldsymbol{u}_B = \boldsymbol{u}_4 - \boldsymbol{u}_1. \tag{3.12}$$

The set of equations (3.11-3.12) completely defines the application of periodic boundary displacements. Equation (2.12) still requires anti-periodic tractions on the boundary. Imposition of the displacements (3.8-3.10) at master and slave nodes induces resulting external forces at these nodes. Furthermore, tying conditions (3.11-3.12) induce tying tractions at the nodes on the boundary. Imposing a zero virtual work at the tied nodes enables to prove that the resulting tying tractions are opposite to each others at every pair of nodes on the boundary (detailed proof in Kouznetsova [51]). Condition (2.12) is thus trivially satisfied.

It should be kept in mind that imposing equations (3.11-3.12) can strongly increase the bandwidth of the system. If a direct solver is used, a much higher computational cost can be expected. On the other hand, using periodic boundary conditions gives better microscopic fields, especially in the surroundings of the inclusions close to the sides of the RVE.

**Computation of the macroscopic response** Computation of the macroscopic stress tensor from the external and tying tractions on the boundary (equation (2.5)) enable to strongly simplify the result (details in Kouznetsova [51]):

$$\bar{\boldsymbol{\sigma}}_{ij} = \frac{1}{V}(t_{1_i} x_{1_j} + t_{2_i} x_{2_j} + t_{4_i} x_{4_j}), \tag{3.13}$$

where $\boldsymbol{t}_1$, $\boldsymbol{t}_2$ and $\boldsymbol{t}_4$ are the resulting external tractions at the master and slave nodes.

This approach is limited to moderate strain/stress gradients otherwise the scale separation hypotheses ($d \ll l$, see figure 2.1) does no apply anymore. In this case, highly localized deformation might occur and precision of the classical FE method cannot be guaranteed. This led to the development of the second-order computational homogenization method which takes into account of the gradient of the macroscopic deformation gradient tensor into the scale transition procedure (Kouznetsova *et al.* [52, 53]). This approach gives an higher-order constitutive response without additional assumptions at the macroscopic level.

## 3.2 Three-dimensional unit cells

In this section, generation of three-dimensional unit cells reinforced by similarly-shaped, non-overlapping and randomly dispersed ellipsoids of revolution is examined. At first, generation of the geometry and the mesh as well as the application of the boundary conditions are presented and followed by an analysis of the unit cell (homogeneity, isotropy, required minimum number of inclusions).

### 3.2.1 Generation of the geometry

For inclusions aligned with their revolution axis and a constant aspect ratio $Ar$, the considered unit cell is a parallelepiped of size $(ArL \times L \times L)$ in order to have the same number of inclusions in all directions. If they are randomly oriented, a cubic unit cell is considered.

At first, the size of the inclusions must be defined (same size is considered for all of them). For a given volume fraction of inclusions $v_1$ and a number of aligned inclusions $N$ within the cell (see in section 3.2.4 how to fix $N$), dimensions of all the ellipsoids' semi-axes can be easily found. Semi-axis length along the revolution axis is $r \times Ar$, while the other two semi-axes have the same length $r = L(3v_1/4\pi N)^{1/3}$. For randomly oriented inclusions, the semi-axis length is: $r = L(3v_1/4\pi NAr)^{1/3}$.

The final particle arrangement must be non-overlapping and suitable for finite element discretization. Similarly to unit cells filled with spheres, the Random Sequential Adsorption (RSA) algorithm (Widom [106]) is used to generate sequentially the coordinates of the particle centers. For this, consider a new particle $E_i$ with a randomly generated center (and orientation if needed). Geometric and discretization conditions that $E_i$ must verify in order to be accepted are:

1. Minimum distance between ellipsoid $E_i$ and all the previously generated ellipsoids.

2. Surface of particle $E_i$ should not be too close to the unit cell faces, edges or corners to prevent the presence of distorted finite elements during meshing.

The minimal distance between two ellipsoids is computed with an iterative algorithm proposed by Lin and Han [63]. As illustrated in 2D on figure 3.4, consider that the minimal distance between ellipsoids $E_1$ and $E_2$ must be determined. At the $k^{th}$ iteration, the two closest points are: $x(k) \in \partial E_1$ and $y(k) \in \partial E_2$, where $\partial E$ means 'the boundary of $E$'. A ball $B(c_1, r_1)$ is constructed completely inside the ellipsoid $E_1$ and tangent to $E_1$ at $x(k)$, and a ball $B(c_2, r_2)$ completely inside the ellipsoid $E_2$ and tangent to $E_2$ at $y(k)$. If the line segment $[c_1, c_2]$ between the two centers is entirely contained in $E_1$ U $E_2$, then the two ellipsoids have a nonempty intersection and the distance $d(E_1, E_2) = 0$; otherwise, the new point $x(k+1)$ is found as the intersection of the line segment $[c_1, c_2]$ with the boundary $\partial E_1$, and the new point $y(k+1)$ as the intersection of the same segment with the boundary $\partial E_2$. Convergence is achieved once the angle between the segment $[x(k+1), y(k+1)]$ and the segment $[c_1(k+1), x(k+1)]$ is smaller than a given tolerance ($c_1(k+1)$ is the center of the new ball tangent to the ellipsoid at $x(k+1)$). A similar test holds for the second ellipsoid. Convergence of the method is guaranteed to the unique solution of the problem. If the minimal distance between the two ellipsoids is

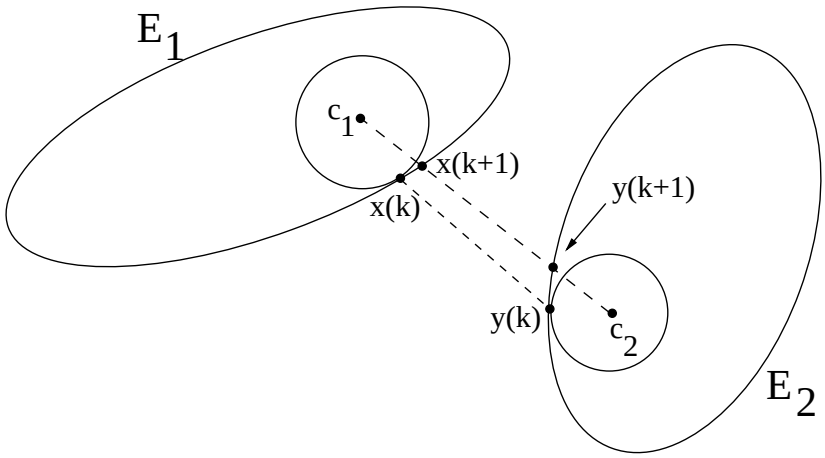


Figure 3.4: One iteration of the algorithm to find the minimal distance between two ellipsoids.

smaller than a given value (typically $3.5\,10^{-2} \times Ar \times r$), this ellipsoid must be rejected.

The second condition is the imposition of a minimal distance between the ellipsoid and faces, edges and corners of the parallelepiped; i.e., the distance has to be checked with respect to planes, lines and points. For the distance between an ellipsoid and a plane, an analytical formula is available ([91]). The other two tests are checked by a modification of the iterative algorithm presented above. If the ellipsoid is too close to a face (or an edge, or a corner) or just slightly crosses it, it must be rejected. Commonly used tolerance for this minimal distance is $5\,10^{-2} \times Ar \times r$. An example of such unit cell generation is illustrated on figure 3.5 for aligned inclusions.

The main limitation of this approach is that only moderate volume fractions of inclusions can be reached. These are reported in table 3.1 for typical values of N and tolerances. For higher volume fractions, Segurado and LLorca [92] proposed an algorithm for sphere reinforced unit cells which enables to reach up to 50% of inclusions. This can be easily extended to ellipsoid-reinforced unit cells. Anyway, for the composites studied in this work, such extension is not required.

### 3.2.2 Mesh generation

If periodic boundary conditions are applied (section 3.1.3), the microstructure must also be periodic so that particles which cut faces of the unit cell are split into the appropriate number of parts (two parts if across one face, four if

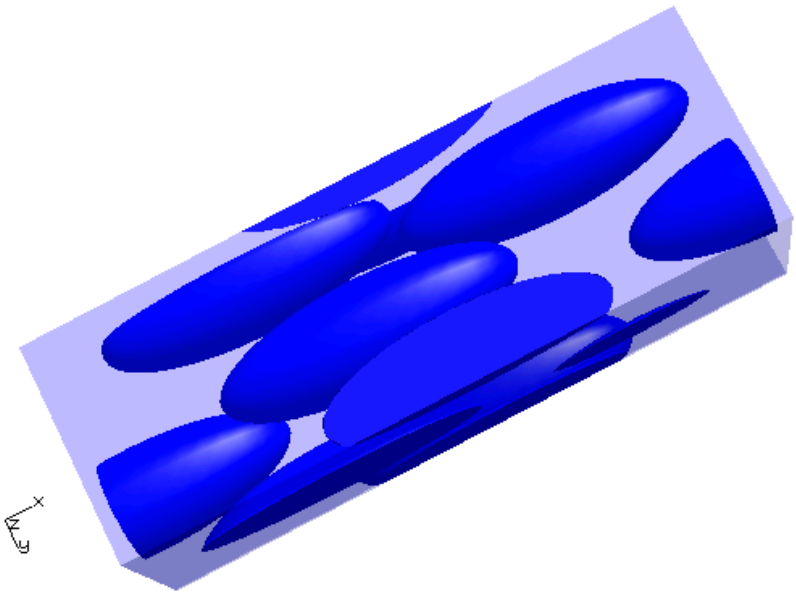

Figure 3.5: Unit cell containing 25% of aligned inclusions (N=5, Ar=3).

| | $v_1$ max. [%] | | |
|---|---|---|---|
| $Ar$ | aligned | 2D random | $v_1$ 3D random |
| 1 | 36 | 36 | 36 |
| 3 | 28 | 28 | 26 |
| 5 | 26 | 20 | 18 |
| 10 | 20 | 12 | 10 |

Table 3.1: Maximum volume fraction of inclusions ($v_1$) reached with the RSA algorithm for various aspect ratios of 30 aligned, 2D randomly dispersed and 3D randomly dispersed inclusions. Typical tolerances on the minimal distances are used.

across two, eight if across three) and copied on the opposite side. The unit cell is meshed with second-order tetrahedra by the software NETGEN [72]. This mesher has very good optimizing properties so that the number of distorted elements is reduced to only a few (less than 5). It also enables to deal with periodic boundary conditions. If the distance between two inclusions is close to the imposed limit, the mesh is refined in this region in order to generally

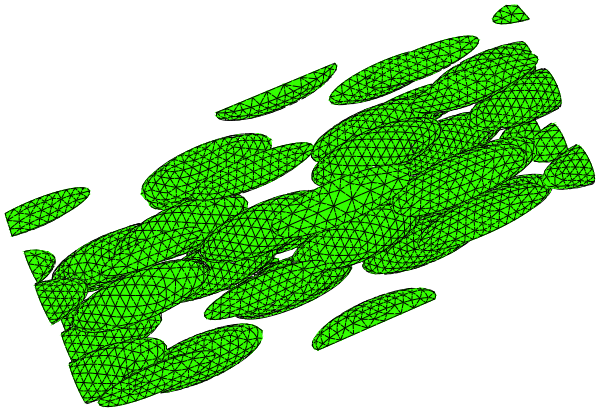

Figure 3.6: Unit cell containing 25% of meshed inclusions.

have a minimum of two elements between these two heterogeneities. Resolution of the problem is done with ABAQUS [1] and 10-node modified tetrahedron (C3D10M) elements are used. Additional degrees of freedom offered by this modified element capture the deformation gradients better than the classical one. For cells reinforced with 30 spheres, a sufficiently refined mesh contains about 90000 nodes and for the same number of ellipsoids (Ar=3), about 110000 nodes are required. A typical mesh for ellipsoidal inclusions can be seen on figure 3.6.

### 3.2.3 Boundary conditions

Application of boundary conditions and resulting simplifications to compute the response of the material have already been examined in section 3.1.3 for 2D unit cells. This can be easily extended to 3D and will not be developed here.

### 3.2.4 Validation of the unit cell

Three validations of the cells containing ellipsoids ($Ar = 3$) generated by the proposed method are examined. As geometrical tests, homogeneity and isotropy of the cell are analyzed. Determination of the minimal required number of inclusions is also done.

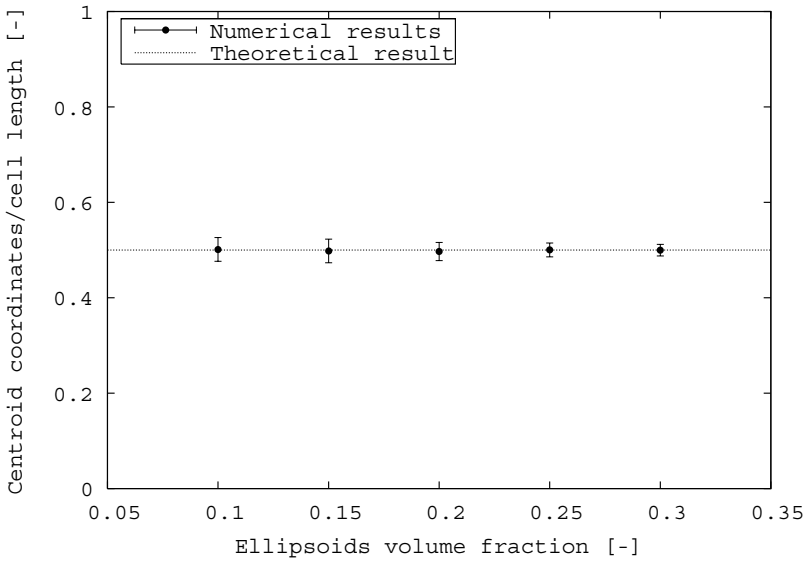


Figure 3.7: Average position and standard deviation of the center of mass of 100 unit cells generated at various volume fractions.

### Geometrical analysis

The first test checks the homogeneity of the generated cells. For several volume fractions of inclusions, 100 cells containing 30 ellipsoids are generated for each of them. For each cell, the position of the center of mass is computed (it is supposed that only inclusions have non-zero density) as well as the average position and standard deviation for a given volume fraction. This is illustrated on figure 3.7. Of course, for a perfectly homogeneous distribution of inclusions, the center of mass should be at the half-length of the cell in each direction. On the figure, the average position always coincides with the reference result while the standard deviation remains very small and logically decreases as the volume fraction of inclusions increases.

In order to check the transverse isotropy of the cell, three moments of inertia with respect to the three perpendicular axes at the center of the cell are computed numerically. For this, the cell is decomposed into many small cubes which have a non-zero mass if they mainly contain part of an ellipsoid. Average and standard deviations with respect to a direction parallel to the revolution axis of the inclusions are plotted on figure 3.8. Theoretical moment of inertia obtained with a homogeneous prism whose mass is equal to the one of the ellipsoids in the random arrangements is given in the direction $x$ by: $v_1 V(L_y^2 + L_z^2)\rho/12$,

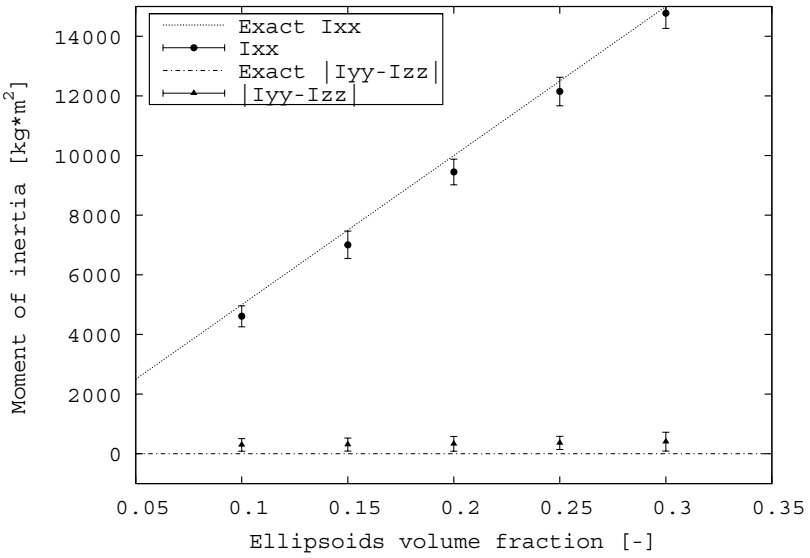


Figure 3.8: Average and standard deviation of the longitudinal (dir. $x$) and transverse (dir. $y$ and $z$) moments of inertia for 100 unit cells generated at various volume fractions $v_1$. $V$ is the volume of the RVE, $L_y$ and $L_z$ the lengths in directions $y$ and $z$ of the RVE and $I_{yy}$ and $I_{zz}$ the moments of inertia with respect to axes $y$ and $z$.

where $\rho$ is the density of the inclusions (considered as equal to one). This result is also reported on the figure and a good agreement is found with numerical results. In addition, for each cell, the moments of inertia with respect to the two others axes should be the same. Their difference in absolute value is also plotted on the figure and remains very small.

These two tests thus show that our method used to generate unit cells containing ellipsoids gives homogeneous and transversely isotropic cells for a wide range of volume fractions of inclusions.

### Numerical analysis

A crucial issue for the accuracy of the FE predictions is to determine the required minimum number of inclusions $N$ within the unit cell. Advantage of small $N$ is that a lower number of elements is required during meshing so that simulations are faster. On the other hand, as we will see, a too small $N$ does not lead to accurate enough predictions. In order to find a compromise, two tests are made. For these, an elasto-plastic matrix ($J_2$ constitutive model

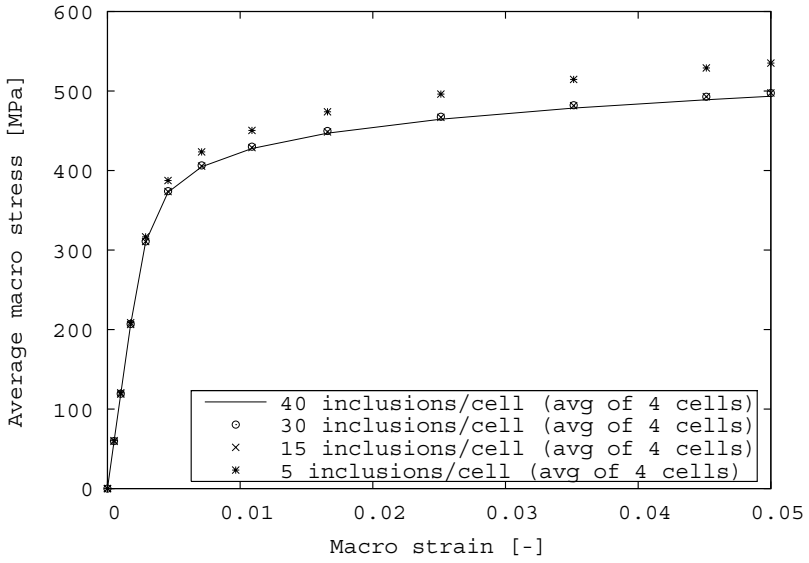


Figure 3.9: FE average response of 4 unit cells for a various number of inclusions within the unit cell. The loading direction is aligned with the ellipsoids.

(see section 5.1), $E = 70$ GPa, $\nu = 0.33$, $\sigma_Y = 1.5924$ MPa, $k = 400$ MPa and $n = 0.05$) is reinforced by elastic inclusions ($E = 400$ GPa and $\nu = 0.2$). All cells contain 25 % of randomly located aligned ellipsoids ($Ar = 3$) and the uniaxial tension direction is along the revolution axis of the ellipsoids.

A first test illustrated on figure 3.9 checks the accuracy of the FE average response obtained for several values of $N$ (5, 15, 30 or 40 inclusions), 4 cells being generated for each $N$. Of course, even for a small $N$, the average response on dozens of different cells would increase the accuracy of the average response but an excessive computation time would be needed. Clearly, 5 inclusions within each cell are not enough since the obtained response is quite far from the reference value (the one corresponding to 40 inclusions). Logically, increasing $N$ reduces this error, the response obtained with 15 inclusions being already very good.

A second test, and maybe even more crucial, is to check the standard deviation of the responses obtained for the different values of $N$. Again, 4 unit cells are generated for each $N$ and results are reported on figure 3.10. As expected, a high scattering is observed (up to 5% of the average value) for a low number of inclusions while this reduces as $N$ increases, the standard deviation for 30

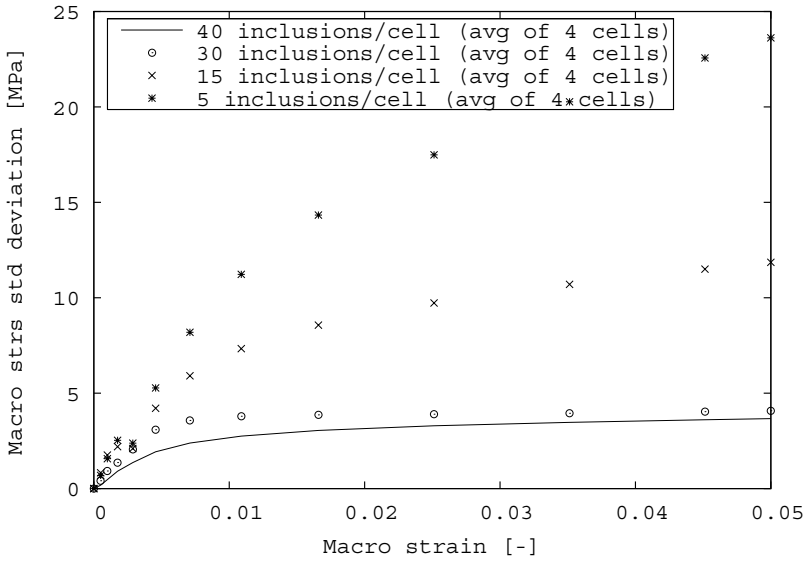


Figure 3.10: FE standard deviation of the average response of 4 unit cells for a various number of inclusions within the cell. The loading direction is aligned with the ellipsoids.

inclusions being already very low.

The analysis of average and standard deviations of FE responses shows that a low number of inclusions leads to an inaccurate average response and a too high standard deviation. For these reasons, we advise to use 30 inclusions within each cell. For such value, corresponding meshes have about 110.000 nodes and 75.000 elements. Mesh refinement has also been successfully checked against a refined one containing more than 200.000 nodes.

## 3.3 Conclusions

In this chapter, we used the finite element method to solve the boundary value problem defined on a representative volume element of heterogeneous materials. For this, various unit cells are proposed, including 2D, 2D axisymmetric and 3D ones. For random distribution of the inclusions, 3D cells with randomly dispersed ellipsoids are generated and meshed with second order tetrahedron. Homogeneity and isotropy of these cells have been checked. Finally, the application of different boundary conditions has been examined. Periodic boundary conditions are studied in depth since they are known to give the most accurate

macroscopic and microscopic predictions. In addition, imposition of these conditions to parallelipipedic cells and computation of the macroscopic response can be done in a simplified way. When using 3D cells and periodic boundary conditions, a minimum of 30 ellipsoidal inclusions (Ar=3.) within the cell has been adopted in order to limit the standard deviation of the macroscopic response obtained with different cells.